Talanta 259 (2023) 124520

Contents lists available at ScienceDirect

Talanta

journal homepage: www.elsevier.com/locate/talanta

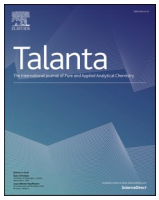

Multifunctional carbon dots for glutathione detection and Golgi imaging

Aikun Liu, Haojie Cai, Zhibing Xu, Jinlei Li, Xiaoyu Weng, Changrui Liao, Jun He, Liwei Liu, Yiping Wang, Junle Qu, Hao Li ***, Jun Song **, Jiaqing Guo *

State Key Laboratory of Radio Frequency Heterogeneous Integration(Shenzhen University); College of Physics and Optoelectronic Engineering, Key Laboratory of Optoelectronic Devices and Systems of Ministry of Education and Guangdong Province, Shenzhen University, Shenzhen, 518060, PR China

ARTICLE INFO

Keywords:
Orange-red fluorescence carbon dots
GSH detection
Golgi imaging

ABSTRACT

Glutathione (GSH) is present in almost every cell in the body and plays various integral roles in many biological processes. The Golgi apparatus is a eukaryotic organelle for the biosynthesis, intracellular distribution, and secretion of various macromolecules; however, the mechanism of GSH in the Golgi apparatus has not been fully elucidated. Here, specific and sensitive sulfur-nitrogen co-doped carbon dots (SNCDs) with orange-red fluorescence was synthesized for the detection of GSH in the Golgi apparatus. The SNCDs have a Stokes shift of 147 nm and excellent fluorescence stability, and they exhibited excellent selectivity and high sensitivity to GSH. The linear response of the SNCDs to GSH was in the range of 10–460 μM (LOD = 0.25 μM). More importantly, we used SNCDs with excellent optical properties and low cytotoxicity as probes, and successfully realized golgi imaging in HeLa cells and GSH detection at the same time.

1. Introduction

Biothiols play a greater role in the physiological activities of humans, and changes in their concentration may be related to many diseases and cell functions. As the richest biological mercaptan in cells, GSH is closely related to biological processes [1]. As an endogenous antioxidant, GSH directly participates in neutralizing reactive oxygen species and free radicals to maintain the balance of the immune system in cells. It also plays important roles in metabolism, cell regulation, and intracellular signal transduction [2–5]. However, GSH abnormalities are closely related to the occurrence of many diseases, such as liver injury, cancer, aging, neurodegenerative diseases, growth retardation, and vascular diseases [6–9]. GSH synthesized in the cytoplasm is distributed in all subcells; including the mitochondria, nucleus, and endoplasmic reticulum. The specific requirements and functions of GSH in various environments are important [10,11]. For example, in the mitochondria, GSH plays a pivotal role in preventing respiratory-induced reactive oxygen species and detoxifying lipid hydroperoxide and electrophilic reagents [12]. In the nucleus, GSH maintains DNA repair and plays a catalytic role in the processes of expression and synthesis [13]. In the endoplasmic reticulum, GSH mainly exists in the form of oxidized glutathione (GSSG), providing the necessary environment for the folding of new proteins and the formation of disulfide bonds [14]. In contrast, the demand and functional impact of GSH in the Golgi apparatus have not been widely studied.

The Golgi apparatus is an organelle found in the majority of eukaryotic cells, and it is the main collection and delivery station that receives protein products from the endoplasmic reticulum. It also participates in lipid transport and lysosomal formation [15,16]. Structural and functional abnormalities of the Golgi apparatus can lead to a range of diseases, including cancer, neurodegenerative disorders, cardiovascular diseases, stroke, and pulmonary hypertension [17–22]. Thus, identifying a specific and sensitive technique to detect GSH in the Golgi apparatus. Rong et al. successfully synthesized a GT-GSH probe, that could target the Golgi apparatus and detect GSH Changes in GSH concentration in the Golgi apparatus, which can be used to study the oxidative stress process of Golgi apparatus [23]. Organic small-molecule dyes are known to have poor resistance to photobleaching and are not suitable for long-term observation. Therefore, a probe with good stability and strong photobleaching resistance must be developed to observe the effect of GSH concentration in the Golgi apparatus.

Carbon quantum dots (CDs), as a new form of fluorescent probe material, have the advantages of high water solubility, good biocompatibility, low toxicity, and high light stability; thus, they have been

* Corresponding author.
** Corresponding author.
*** Corresponding author.
E-mail addresses: lihao000000@163.com (H. Li), songjun@szu.edu.cn (J. Song), 523986726@qq.com (J. Guo).

https://doi.org/10.1016/j.talanta.2023.124520
Received 30 December 2022; Received in revised form 30 March 2023; Accepted 31 March 2023
Available online 6 April 2023

widely used in the field of biosensors and biological imaging [24–29]. Although targeting CDs have been used to detect GSH in subcellular organelles (including lysosomes and mitochondria), targeted Golgi CDs for the detection of glutathione have not been reported [30–32]. Therefore, multifunctional CDs should be developed, which can accurately and sensitively locate Golgi apparatus and monitor changes of GSH concentration.

To solve the above problems, we used o-phenylenediamine and phenyl-sulfonamide as precursors to synthesize SNCDs with orange light using one-step hydrothermal method. SNCDs exhibit ultra-low toxicity, excellent biocompatibility, and high stability. This probe can sensitively detect GSH in solution and has excellent targeting effect on the Golgi apparatus. SNCDs as the probe can support the detection and visualization of exogenous GSH in Golgiin HeLa cells.

2. Methods

2.1. Preparation of the SNCDs

Scheme 1 describes the preparation process, in which 3 mmol of o-phenylenediamine, 2 mmol of benzenesulfonamide, and 30 mL of ultrapure water were added to the polytetrafluoroethylene lining. The mixture was heated at 180 °C for 9 h under static conditions in a stainless-steel autoclave. After cooling to room temperature, a yellow-brown solution was obtained and large particles were removed through a 0.22 μm needle filter. The above solution was placed in 500 Da dialysis bag for dialysis to remove small molecular impurities, and then freeze-drying was performed to obtain SNCDs.

2.2. Preparing for SNCDs-based testing

SNCDs were dispersed in ultra-pure water to obtain a 3 mg/mL SNCD solution. Then, 100 μL (3 mg/mL) of the SNCDs solution was added to 3 mL water, and 100 μg/mL of the SNCDs solution was collected for the spectral test.

2.3. Cellular toxicity test

HeLa cells were placed in culture flasks (Nunc, T25 EasY Flash), added to complete DMEM culture medium (DMEM: FBS = 10:1), and incubated in a cell culture chamber at 37 °C. Dilute the cells after digestion and centrifugation, and the cell suspension was added to 96 well plates and incubation for 24 h. Then, different concentrations of SNCDs were added and incubated for 24 h. After incubation, each well was washed twice with PBS. CCK-8 was mixed with the culture solution at 1:10, and 100 μL was added to each well. After reacting for 1 h, the optical density (OD) at 450 nm was obtained on the microplate reader.

2.4. Cell imaging

The HeLa cell line is used as a model for SNCDs imaging.1 mL of DMEM medium containing SNCDs (without FBS) was added to the cell culture dish and incubated in the cell incubator for 30 min. Then, incubate cells with a commercial Golgi Tracker Green probe according to the instructions to verify the targeting ability of SNCDs to Golgi apparatus. The cell line was rinsed three times with PBS to remove the residual probe, and imaging was performed using Nikon A1R MP+ laser scanning confocal fluorescence microscopy. The excitation wavelengths of SNCDs and Golgi-Tracker Green probes are 405 nm and 488 nm, respectively.

3. Results and discussion

3.1. SNCDs characteristics

Here, the morphology, size, structure, element composition, and optical properties of the prepared SNCDs were characterized and analyzed by different technical means. Firstly, the morphology and size of the TEM image (Fig. 1a) showed that SNCDs are spherical and uniformly dispersed. The average particle size is 2.43 nm, distributed in the range of 1.75 nm–3.25 nm (Fig. 1b). Next, we characterized the surface functional groups of SNCD by FTIR (Fig. 1c). –OH and –NH_2 stretching vibrations are identified from the absorption peaks at 3446–3225 cm^{-1} [33]. The absorption peak at 1635 cm^{-1} is attributed to the stretching vibration of C=O. The absorption peak at 1581 cm^{-1} and 1448 cm^{-1} correspond to C–C and C–N stretching vibrations [34,35]. The tensile vibrations of C–O, C–S, and C–H are identified from the peaks within 1000–1350 cm^{-1} [36,37]. C–O–C stretching vibrations corresponded to the 1448 cm^{-1} absorption bands [34]. And, the peaks observed at 899, 753, and 684.3 cm^{-1} originate from the stretching vibrations of the bending modes of S=O, S–O, and S–C, respectively [38]. The FTIR analysis showed that the SNCDs was modified with amino, carboxyl, sulfonamide groups, and sulfonic acid residues. X-ray photoelectron spectroscopy (XPS) showed four peaks at 284.8, 398.8, 532.1, and 167.9 eV (Fig. 1d), which corresponded to C 1s, N 1s, O 1s, and S 2p, respectively. The results indicated that the prepared SNCDs were doped with heteroatoms (N and S). The high-resolution C 1s XPS spectrum (Fig. 1e) revealed the existence of various carbon-bonded substances, such as C–C/C=C (284.8 eV), C–N/C–S (286.1 eV) and –COOH (288.6 eV) [26, 39]. In the high-resolution spectrum of N 1s, O 1s, and S 2p, pyridine nitrogen, amino nitrogen, and pyrrole correspond to peaks at 398.5 eV, 399.1 eV, and 399.84 eV, respectively (Fig. 1f); C–OH, C–O–C, C=O, and O=C–O correspond to the characteristic peaks of O is at 531.2, 531.9, 532.5 and 533.2 eV, respectively (Fig. S1); The S 2p spectrum (Fig. 1g) showed that the peaks at 167.7 and 169.2 eV corresponded to the

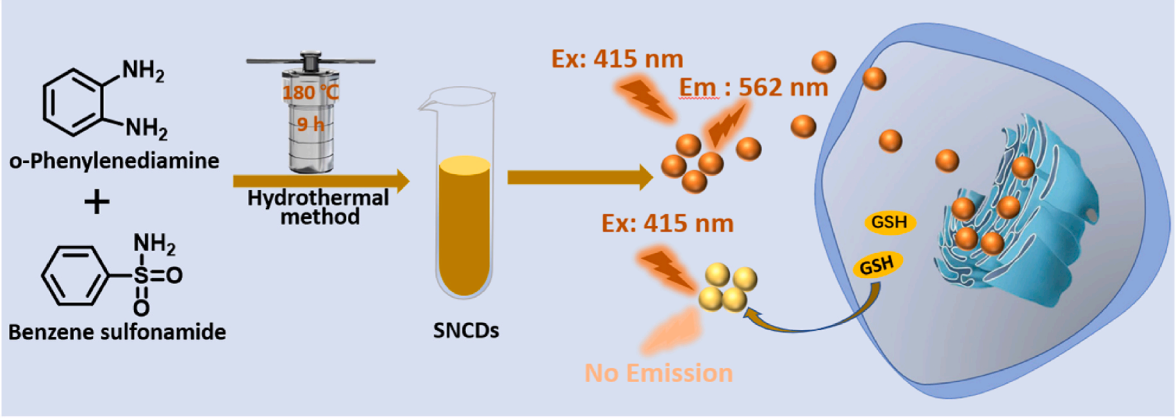

Scheme 1. Synthesis of the SNCDs and design for detecting GSH in the Golgi apparatus.

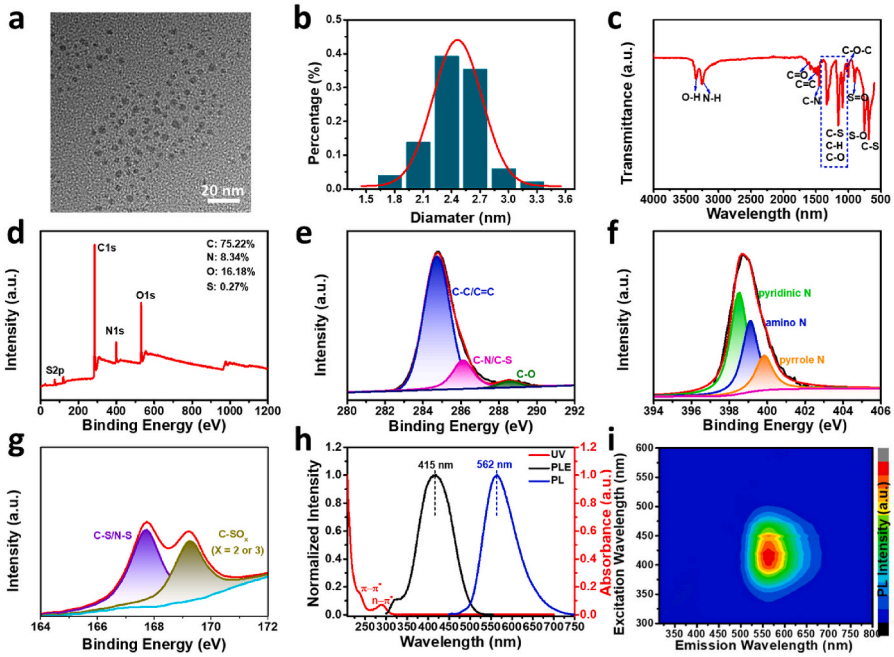

Fig. 1. Characterization of SNCDs (a) TEM image; (b)size distribution; (c) FTIR spectrum; (d) full XPS spectrum; (e–g) high-resolution XPS spectra of C 1s; N 1s; S 2p; (h) UV–Vis absorption spectrum (red curve), excitation spectrum (black curve) and emission spectrum (blue curve); and (i) 3D spectrum of the SNCDs.

C–S/N–S and C–SO_X (X = 2 and 3) sulfur groups [40–43]. Therefore, we proved that the surfaces of the prepared SNCDs are mainly filled with amino, carboxyl, and sulfonamide groups.

In addition, the UV–Vis absorption and photoluminescence spectra of SNCDs were studied. As shown in Fig. 1h, the two absorption bands of the UV–Vis absorption spectrum at 238 nm and 274 nm (red curves) correspond to the aromatic sp^2 domain of the π-π* transition of the C=C bond and the n–π* transition of the C=O/C–N bond, respectively. These results show that the SNCDs have a highly conjugated structure [33]. The optimal excitation wavelength (λ_{Ex} = 415 nm) and emission wavelength (λ_{Em} = 562 nm) are shown in black and blue lines, respectively. Next, the relationship between the excitation and emission of SNCDs was studied. As shown in Fig. 1i and Fig. S2, both the 3D spectrum and fluorescence spectrum showed that the fluorescence emission spectra of the SNCDs were independent of the excitation spectra, and all the emission were located at 562 nm, showing bandgap luminescence. The absolute fluorescence quantum yield of the SNCDs measured using the fluorescence spectrometer is 9.08%.

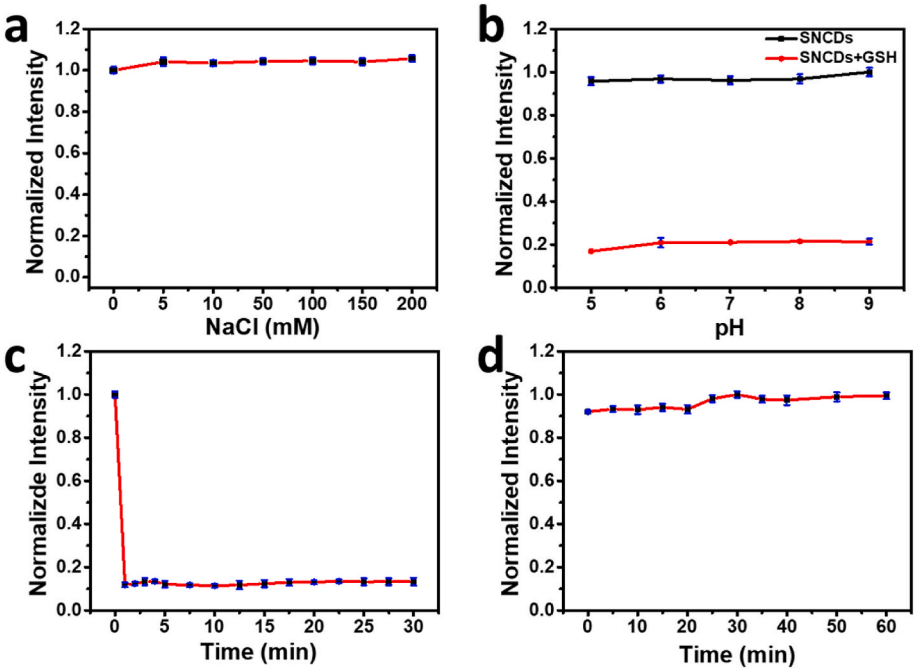

Fig. 2. Normalized fluorescence intensity of the SNCDs based on the following conditions: (a) NaCl solution with a concentration of 0–200 mM; (b) fluorescence intensity without GSH (red) and with GSH (black) under different pH conditions; (c) relationship between fluorescence quenching and time in presence of GSH (1 mM); and (d) fluorescence intensity at different irradiation times.

3.2. SNCDs stability

Here, the chemical and optical stabilities of the SNCDs as sensing probes in different environments are discussed. First, we studied the photostability of the SNCDs in NaCl solutions of different concentrations. Fig. 2a shows that the fluorescence intensity of the SNCDs is stable in the NaCl concentration range of 0–200 mM. As shown in Fig. 2b, within the physiological pH range of 5–9, the SNCDs showed excellent photostability and responsiveness to GSH. Fig. 2c shows the response speed and stability of the SNCDs to GSH. After adding GSH (1 mM) to the SNCDs solution, the fluorescence was quenched rapidly within 1 min and remained stable for 30 min. Therefore, the test was performed within 1min of the solution preparation. Fig. 2d shows that after the SNCDs were irradiated by ultraviolet light (365 nm) for 1 h, the fluorescence intensity was almost unchanged, indicating that SNCDs have excellent resistance to photobleaching.

3.3. SNCDs selectivity

Next, we tested the selectivity of the SNCDs for the detection of GSH by independently measuring the fluorescence response of the SNCDs to different ions, biological mercaptans, and amino acids (e.g., GSH, Na^+, Ca^{2+}, Zn^{2+}, Cu^{2+}, Mg^{2+}, Fe^{3+}, Ag^+, Ba^{2+}, Li^+, Mn^{2+}, Pb^{2+}, Cl^-, Br^-, F^-, NO_2^-, NO_3^-, HS^-, SO_4^{2-}, SO_3^{2-}, SCN^-, HCO_3^-, CO_3^{2-}, HPO_4^{2-}, $H_2PO_4^-$, $H_2PO_2^-$, Cys, Hcy, His, Trp, Gly, Phe, and Lys). Fig. 3a shows a comparison of the fluorescence response of the SNCDs and indicates that only the addition of GSH caused fluorescence quenching. Fig. 3b shows that the effect of adding ions, biological mercaptans, and amino acids to the solution of GSH-quenched SNCDs fluorescence is negligible, thus indicating that GSH detection by SNCDs was not disturbedby the ions, biological mercaptans, and amino acid.

3.4. Photoluminescent quenching

Fig. 4a shows the relationship between the concentration of GSH and the fluorescence intensity of the SNCDs.The position of the emission peak of the SNCDs will not be changed during quenching after adding GSH, indicating that the energy band structure of the SNCDs did not change [44]. As shown in Fig. 4b, through the linear fitting, the

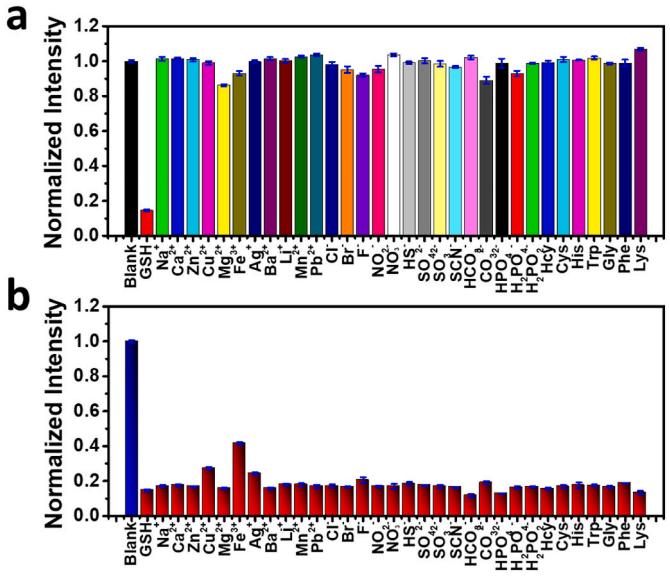

Fig. 3. Normalized fluorescence intensity (a) selectivity of the SNCDs for GSH (1 mM) over other ions, biological mercaptans, and amino acids (1 mM); (b) interference of the SNCDs after adding the mixture of GSH(1 mM) and other ions, biological mercaptans, and amino acids (1 mM).

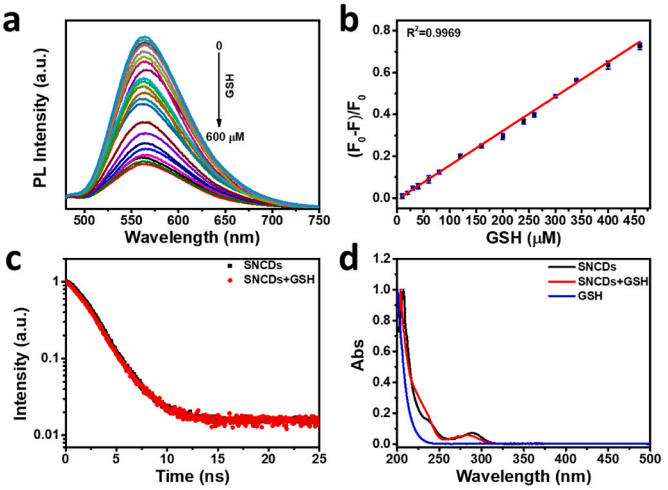

Fig. 4. (a) FL spectra of the SNCDs at different concentrations of GSH; (b)the relationship between $(F_0–F)/F_0$ and glutathione concentration (10–460 μM); (c) FL decay curves of the SNCDs and SNCD-GSH; and (d) UV–vis absorption of the SNCDs, GSH, and SNCD-GSH solutions.

fluorescence intensity in the range of 10–460 μM was linearly correlated with the concentration of GSH ($R^2 = 0.9969$). According to the rule of "triple standard deviation", the LOD of the detection system was 0.25 μM [45]. In addition, a comparison of the linear range and detection limit with the results in the literature indicated that the SNCDs showed a wider detection range and lower LOD about GSH concentrations (Table S1) [46–53].

Next, we discuss the quenching mechanism of the SNCDs after adding GSH. The reported fluorescence quenching mechanisms mainly include dynamic quenching, static quenching, Förster resonance energy transfer (FRET), photoinduced electron transfer (PET), and internal filtering effect (IFE) [54]. Fig. 4c shows the fluorescence lifetimes of the SNCDs and SNCD-GSH. The fluorescence lifetime of the SNCDs changed from 2.378 ns to 2.324 ns after the addition of GSH, which can be considered almost unchanged after adding GSH. Next, we compared the absorption spectra of the SNCDs and SNCD-GSH (Fig. 4d). After adding GSH to the SNCDs solution, the absorption peak changed from 289.9 nm to 282.4 nm, indicating that GSH statically quenched the SNCDs.

In the static quenching mechanism, the fluorophore and quenching agent form a ground-state complex [55–57]. The zeta potential was further tested (Fig. S3). When GSH was added to the SNCD solution, the potential changed from −13.70 to 21.23 mV, indicating that the surface functional group GSH was bound. Fig. S4 shows that the emission peaks of the SNCDs and SNCDs-GSH are in the same position, indicating that SNCDs and GSH form non-covalent bonds. In Figs. S5–S6, the changes in the FRTE and XPS spectra further indicate that GSH is combined with SNCDs. The above results indicate that GSH quenching of the SNCDs is a static fluorescence quenching process.

3.5. Cellular imaging

SNCDs exhibit excellent stability and optical properties, and thus may be suitable for cell imaging experiments. We performed a CCK-8 assay to study the cytotoxicity of the SNCDs (Fig. 5a). HeLa cells were incubated with SNCDs at a concentration of 400 μg/mL for 24 h, and the cell activity was more than 98%. The results indicate that the toxicity of the SNCDs can be ignored, which is suitable for imaging detection of living cells. The Golgi apparatus is a part of the inner membrane of eukaryotic cells, which is used to synthesize and secrete various cellular macromolecules. The development of a Golgi fluorescent probe is of great significance for studying its morphological changes and related physiological processes [24]. After HeLa cells were stained with SNCDs,

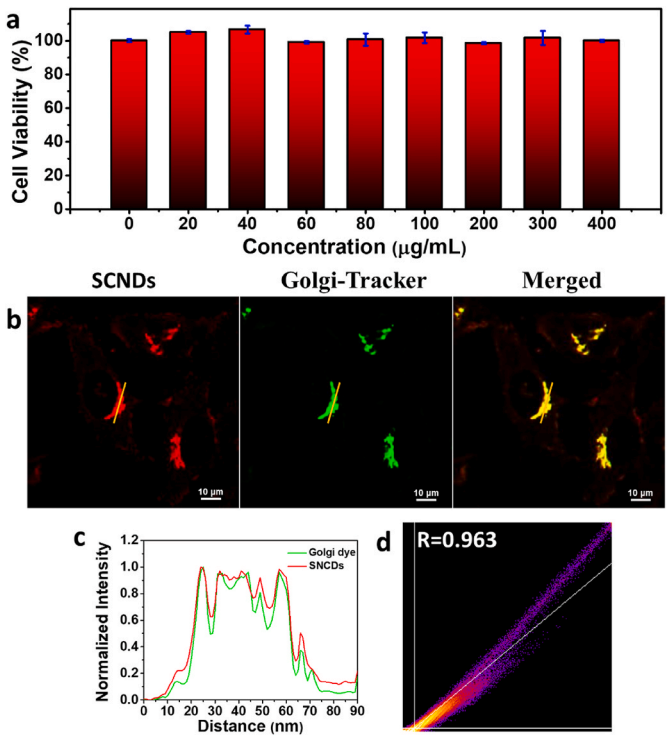

Fig. 5. (a)Relationship between HeLa cell viability and SNCDs concentration; (b) fluorescence imaging and co-localization of the SNCDs and Golgi-Tracker Green probe in HeLa cells; (c) normalized intensity distribution map of the same linear region in SNCDs and Golgi-Tracker Green probe images; and (d) Pearson correlation coefficient of combined images (R = 0.963).

CLSM imaging showed that most SNCDs were enriched in the Golgi region of the cells. To further verify the targeting of the SNCDs to Golgi, co-localization experiments with commercial Golgi-Tracker Green were conducted. HeLa cells were incubated with SNCDs and Golgi Tracker Green, and then confocal imaging was performed using 405 nm and 488 nm excitation channels, respectively (Fig. 5b), and overlapped. Fig. 5c shows that the fluorescence distribution intensity of the two probes in HeLa cells overlapped significantly. Based on the image overlapping, and the results showed that the co-location coincidence rate is as high as 96.3% (Fig. 5d). SNCDs show good biocompatibility and excellent targeting, thus indicating that they are potential candidates for the development of new commercial Golgi probes.

To verify the recognition ability of the SNCDs to intracellular GSH, HeLa cells were incubated with the SNCDs (150 μg/mL) for 30 min and then imaged. Fig. 6a–c shows the accumulation of fluorescent signals in the Golgi apparatus. After adding 5 mM exogenous GSH solution to the above cells, the intracellular fluorescence intensity was quenched (Fig. 6d–f). The results showed that SNCDs could detect GSH in living cells. A comparison of the enlarged portion in Fig. 6 shows that the fluorescence intensity of the Golgi apparatus decreased significantly after the addition of GSH and the distribution morphology changed. This indicates that the concentration of GSH affects the Golgi apparatus. Next, the responsiveness of the SNCDs to different concentrations of exogenous GSH in HeLa cells was verified. Figs. S7a–c shows confocal images of control cells incubated with SNCDs only. Then, the two batches of HeLa cells were incubated with different concentrations of GSH. 5 mM GSH was added to the cells for incubation for 30 min, and then SNCD (150 μ g/ml) was added for 30 min (Figs. S7d–f). Next, as previously mentioned, cells incubated with 10 mM GSH were imaged (Figs. S7g–i). It can be seen that with the increase of GSH concentration in cells, the fluorescence becomes weaker when SNCDs solution of the same concentration was added. The results showed that SNCDs could be used for the qualitative detection of GSH in cells, which was consistent with that in vitro.

4. Conclusions

In conclusion, we have successfully obtained Golgi-targeted carbon dots (SNCDs) with orange-red fluorescence by a one-step hydrothermal method and doping effect. These SNCDs exhibited excellent water solubility, outstanding optical stability, high selectivity, and sensitivity to GSH. SNCDs have the advantages of low cost, high sustainability, short response time, low detection limit (0.25 μM), and wide detection range (10–460 μM), which make them excellent fluorescent probes for evaluating GSH. SNCDs also exhibit good biocompatibility, low cytotoxicity, and good Golgi targeting, which enables the detection of GSH while performing Golgi targeting imaging. This study provides a new method

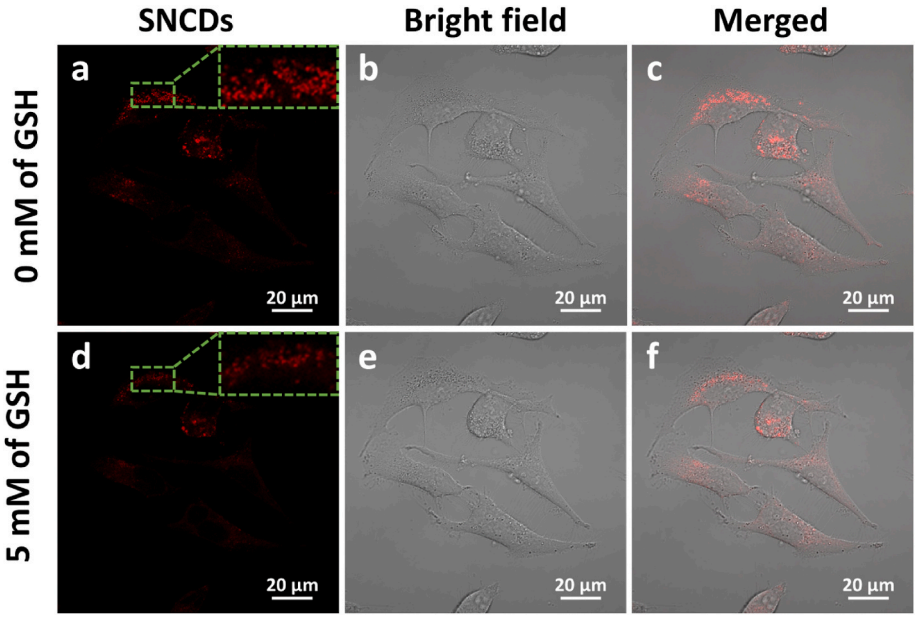

Fig. 6. Confocal images of HeLa cells (a–c) incubated with 150 μg/mL SNCDs for 30 min; and (d–f) 5 mM GSH was added to HeLa cells after incubation with SNCDs solution.

for accurately monitoring the state of the Golgi apparatus and simultaneously monitoring the concentration of glutathione. It may also provide a new tool for early diagnosis of related diseases in the future.

Credit author statement

Aikun Liu: Investigation, Formal analysis, Writing – original draft, Supervision, Writing – review & editing. **Haojie Cai**: Investigation, Writing – review & editing. **Zhibing Xu**: Investigation, Formal analysis. Jinlei Li: Investigation, Formal analysis. **Xiaoyu Weng**: Validation. **Changrui Liao**: Conceptualization. **Jun He**: Software. Liwei Liu: Software, Formal analysis. **Yiping Wang**: Investigation. **Junle Qu**: Supervision Funding acquisition. **Jiaqing Guo**: Validation, Supervision, Funding acquisition. **Hao Li**: Validation, Supervision, Funding acquisition. **Jun Song**: Validation, Supervision, Funding acquisition.

Declaration of competing interest

The authors declare that they have no known competing financial interests or personal relationships that could have appeared to influence the work reported in this paper.

Data availability

Data will be made available on request.

Acknowledgements

This work has been partially supported by the National Key R&D Program of China (2021YFF0502900); National Natural Science Foundation of China (62175161/61835009/62127819), China Postdoctoral Science Foundation (2021M702240). Guangdong Basic and Applied Basic Research Foundation (2023A1515011499/2023A1515011114), Shenzhen Science and Technology Program (JCYJ20210324095810028/JCYJ20210324095613036) and Shenzhen Key Laboratory of Photonics and Biophotonics (ZDSYS20210623092006020). We thank Instrument Analysis Center of Shenzhen University, Photonics Research Center of Shenzhen University and Ph.D. Lin for the technical assistance with the Leica SP8 confocal microscopy instrument.

Appendix A. Supplementary data

Supplementary data to this article can be found online at https://doi.org/10.1016/j.talanta.2023.124520.

References

[1] M. Yang, J. Fan, W. Sun, J. Du, X. Peng, Mitochondria-anchored colorimetric and ratiometric fluorescent chemosensor for visualizing cysteine/homocysteine in living cells and Daphnia magna model, Anal. Chem. 91 (19) (2019) 12531–12537.
[2] A.L. Ortega, S. Mena, J.M. Estrela, Glutathione in cancer cell death, Cancers 3 (1) (2011) 1285–1310.
[3] D. Wang, Y.T. Meng, Y. Zhang, Q. Wang, W.Jj. Lu, S.M. Shuang, C. Dong, A specific discriminating GSH from Cys/Hcy fluorescence nanosensor: the carbon dots-MnO_2 nanocomposites, Sens. Actuators, B 367 (2022), 132135.
[4] W. Dong, R. Wang, X. Gong, C. Dong, An efficient turn-on fluorescence biosensor for the detection of glutathione based on FRET between N,S dual-doped carbon dots and gold nanoparticles, Anal. Bioanal. Chem. 411 (25) (2019) 6687–6695.
[5] V.K. Singh, P.K. Yadav, S. Chandra, D. Bano, M. Talat, S.H. Hasan, Peroxidase mimetic activity of fluorescent NS-carbon quantum dots and their application in colorimetric detection of H_2O_2 and glutathione in human blood serum, J. Mater. Chem. B 6 (32) (2018) 5256–5268.
[6] J. Ly, M. Lagman, T. Saing, M.K. Singh, E.V. Tudela, D. Morris, J. Anderson, J. Daliva, C. Ochoa, N. Patel, D. Pearce, V. Venketaraman, Liposomal glutathione supplementation restores TH1 cytokine response to Mycobacterium tuberculosis infection in HIV-infected individuals, J. Interferon Cytokine Res. 35 (11) (2015) 875–887.
[7] G. Teskey, R. Abrahem, R. Cao, K. Gyurjian, H. Islamoglu, M. Lucero, A. Martinez, E. Paredes, O. Salaiz, B. Robinson, V. Venketaraman, Glutathione as a marker for human disease, Adv. Clin. Chem. 87 (2018) 141–159.
[8] Y. Gao, K. Wu, H. Li, W. Chen, M. Fu, K. Yue, X. Zhu, Q. Liu, Glutathione detection based on peroxidase-like activity of Co_3O_4–Montmorillonitenanocomposites, Sens. Actuators, B 273 (2018) 1635–1639.
[9] R. Wu, H. Ge, C. Liu, S. Zhang, L. Hao, Q. Zhang, J. Song, G. Tian, J. Lv, A novel thermometer-type hydrogel senor for glutathione detection, Talanta 196 (2019) 191–196.
[10] M. Mari, A. Morales, A. Colell, C. Garcia-Ruiz, N. Kaplowitz, J.C. Fernandez-Checa, Mitochondrial glutathione: features, regulation and role in disease, Biochim. Biophys. Acta 1830 (5) (2013) 3317–3328.
[11] Y. Zhou, S. Huang, H. Shen, M. Ma, B. Zhu, D. Zhang, Detection of glutathione in oral squamous cell carcinoma cells with a fluorescent probe during the course of oxidative stress and apoptosis, J. Oral Maxillofac. Surg. 75 (1) (2017) 223 e1–e223 e10.
[12] V. Ribas, C. Garcia-Ruiz, J.C. Fernandez-Checa, Glutathione and mitochondria, Front. Pharmacol. 5 (2014) 151.
[13] M. Valko, D. Leibfritz, J. Moncol, M.T. Cronin, M. Mazur, J. Telser, Free radicals and antioxidants in normal physiological functions and human disease, Int. J. Biochem. Cell Biol. 39 (1) (2007) 44–84.
[14] D.D. Sarkar, S.K. Edwards, J.A. Mauser, A.M. Suarez, M.A. Serowoky, N.L. Hudok, P.L. Hudok, M. Nunez, C.S. Weber, R.M. Lynch, O. Miyashita, T.S. Tsao, Increased redox-sensitive green fluorescent protein reduction potential in the endoplasmic reticulum following glutathione-mediated dimerization, Biochemistry 52 (19) (2013) 3332–3345.
[15] R.S. Li, C. Wen, C.Z. Huang, N. Li, Functional molecules and nano-materials for the Golgi apparatus-targeted imaging and therapy, TrAC-Trend. Analy. Chem. 156 (2022), 116714.
[16] J. Liu, Y. Huang, T. Li, Z. Jiang, L. Zeng, Z. Hu, The role of the Golgi apparatus in disease (Review), Int. J. Mol. Med. 47 (4) (2021).
[17] X. Tan, P. Banerjee, H.F. Guo, S. Ireland, D. Pankova, Y.H. Ahn, I.M. Nikolaidis, X. Liu, Y. Zhao, Y. Xue, A.R. Burns, J. Roybal, D.L. Gibbons, T. Zal, C.J. Creighton, D. Ungar, Y. Wang, J.M. Kurie, Epithelial-to-mesenchymal transition drives a pro-metastatic Golgi compaction process through scaffolding protein PAQR11, J. Clin. Invest. 127 (1) (2017) 117–131.
[18] W.O. Rendon, E. Martinez-Alonso, M. Tomas, N. Martinez-Martinez, J.A. Martinez-Menarguez, Golgi fragmentation is Rab and SNARE dependent in cellular models of Parkinson's disease, Histochem. Cell Biol. 139 (5) (2013) 671–684.
[19] H. Brandstaetter, A.J. Kruppa, F. Buss, Huntingtin is required for ER-to-Golgi transport and for secretory vesicle fusion at the plasma membrane, Dis. Model. Mech. 7 (12) (2014) 1335–1340.
[20] E. Tarazon, E. Rosello-Lleti, A. Ortega, C. Gil-Cayuela, J.R. Gonzalez-Juanatey, F. Lago, L. Martinez-Dolz, M. Portoles, M. Rivera, Changes in human Golgi apparatus reflect new left ventricular dimensions and function in dilated cardiomyopathy patients, Eur. J. Heart Fail. 19 (2) (2017) 280–282.
[21] T. Li, H. You, X. Mo, W. He, X. Tang, Z. Jiang, S. Chen, Y. Chen, J. Zhang, Z. Hu, GOLPH3 mediated golgi stress response in modulating N2A cell death upon oxygen-glucose deprivation and reoxygenation injury, Mol. Neurobiol. 53 (2) (2016) 1377–1385.
[22] J. Lee, R. Reich, F. Xu, P.B. Sehgal, Golgi, trafficking, and mitosis dysfunctions in pulmonary arterial endothelial cells exposed to monocrotaline pyrrole and NO scavenging, Am. J. Physiol. Lung Cell Mol. Physiol. 297 (4) (2009). L715- L728.
[23] X. Rong, C. Liu, M. Li, H. Zhu, Y. Zhang, M. Su, X. Wang, X. Li, K. Wang, M. Yu, W. Sheng, B. Zhu, An integrated fluorescent probe for ratiometric detection of glutathione in the golgi apparatus and activated organelle-targeted therapy, Anal. Chem. 93 (48) (2021) 16105–16112.
[24] F. Lin, C. Jia, F.G. Wu, Carbon dots for intracellular sensing, Small Struct. 3 (9) (2022), 2200033.
[25] X.W. Hua, Y.W. Bao, J. Zeng, F.G. Wu, Nucleolus-targeted red emissive carbon dots with polarity-sensitive and excitation-independent fluorescence emission: high-resolution cell imaging and in vivo tracking, ACS Appl. Mater. Interfaces 11 (36) (2019) 32647–32658.
[26] Y. Jiao, X. Gong, H. Han, Y. Gao, W. Lu, Y. Liu, M. Xian, S. Shuang, C. Dong, Facile synthesis of orange fluorescence carbon dots with excitation independent emission for pH sensing and cellular imaging, Anal. Chim. Acta 1042 (2018) 125–132.
[27] X. Geng, Y. Sun, Z. Li, R. Yang, Y. Zhao, Y. Guo, J. Xu, F. Li, Y. Wang, S. Lu, L. Qu, Retrosynthesis of tunable fluorescent carbon dots for precise long-term mitochondrial tracking, Small 15 (48) (2019), 1901517.
[28] E. Shuang, Q.X. Mao, J.H. Wang, X.W. Chen, Carbon dots with tunable dual emissions: from the mechanism to the specific imaging of endoplasmic reticulum polarity, Nanoscale 12 (12) (2020) 6852–6860.
[29] L. Cao, T. Zhu, M. Zan, Y. Liu, X. Xing, Q. Qian, Q. Mei, W.F. Dong, L. Li, Red emissive N, Cl-doped carbon dots for detection of tea polyphenols and lysosomal imaging at the cellular level, Sens. Actuators, B 370 (2022), 132424.
[30] N. Gong, X. Ma, X. Ye, Q. Zhou, X. Chen, X. Tan, S. Yao, S. Huo, T. Zhang, S. Chen, X. Teng, X. Hu, J. Yu, Y. Gan, H. Jiang, J. Li, X.J. Liang, Carbon-dot-supported atomically dispersed gold as a mitochondrial oxidative stress amplifier for cancer treatment, Nat. Nanotechnol. 14 (4) (2019) 379–387.
[31] T. Wu, X. Liang, X. Liu, Y. Li, Y. Wang, L. Kong, M. Tang, Induction of ferroptosis in response to graphene quantum dots through mitochondrial oxidative stress in microglia, Part, Fibre. Toxicol. 17 (1) (2020) 30.
[32] D. Chang, Z. Zhao, L. Shi, W. Liu, Y. Yang, Lysosome-targeted carbon dots for colorimetric and fluorescent dual mode detection of iron ion, in vitro and in vivo imaging, Talanta 232 (2021), 122423.
[33] H. Li, H. Wang, J. Guo, S. Ye, W. Shi, X. Peng, J. Song, J. Qu, Long-wavelength excitation of carbon dots as the probe for real-time imaging of the living-cell cycle process, Sens. Actuators, B 311 (2020), 127891.

[34] S. Wei, T. Li, X. Zhang, H. Zhang, C. Jiang, G. Sun, An "on-off-on" selective fluorescent probe based on nitrogen and sulfur co-doped carbon dots for detecting Cu(2+) and GSH in living cells, Anal. Methods 12 (42) (2020) 5110–5119.
[35] Z. Song, F. Quan, Y. Xu, M. Liu, L. Cui, J. Liu, Multifunctional N,S co-doped carbon quantum dots with pH- and thermo-dependent switchable fluorescent properties and highly selective detection of glutathione, Carbon 104 (2016) 169–178.
[36] H. Ding, J.S. Wei, H.M. Xiong, Nitrogen and sulfur co-doped carbon dots with strong blue luminescence, Nanoscale 6 (22) (2014) 13817–13823.
[37] Y. Dong, H. Pang, H.B. Yang, C. Guo, J. Shao, Y. Chi, C.M. Li, T. Yu, Carbon-based dots co-doped with nitrogen and sulfur for high quantum yield and excitation-independent emission, Angew Chem. Int. Ed. Engl. 52 (30) (2013) 7800–7804.
[38] X.W. Yu, X. Liu, Y.W. Jiang, Y.H. Li, G. Gao, Y.X. Zhu, F. Lin, F.G. Wu, Rose bengal-derived ultrabright sulfur-doped carbon dots for fast discrimination between live and dead cells, Anal. Chem. 94 (10) (2022) 4243–4251.
[39] J. Kaushik Gunture, A.K. Garg, D. Saini, P. Khare, S.K. Sonkar, Pollutant diesel soot derived onion-like nanocarbons for the adsorption of organic dyes and environmental assessment of treated wastewater, Ind. Eng. Chem. Res. 59 (26) (2020) 12065–12074.
[40] A. Paul, M. Kurian, N-doped photoluminescent carbon dots from water hyacinth for tumour detection, Mater. Today: Proc. 25 (2020) 213–217.
[41] H. Qi, X. Sun, T. Jing, J. Li, J. Li, Integration detection of mercury(ii) and GSH with a fluorescent "on-off-on" switch sensor based on nitrogen, sulfur co-doped carbon dots, RSC Adv. 12 (4) (2022) 1989–1997.
[42] X. Zhang, L. Chen, Y.-Y. Wei, J.-L. Du, S.-P. Yu, X.-G. Liu, W. Liu, Y.-J. Liu, Y.-Z. Yang, Q. Li, Cyclooxygenase-2-targeting fluorescent carbon dots for the selective imaging of Golgi apparatus, Dyes Pigments 201 (2022), 110213.
[43] K. Huner, F. Karaman, A novel n-type poly(sulfonic acid diphenyl aniline) and its nanocomposites with large Seebeck coefficient enhanced with external magnetic fields, J. Appl. Polym. Sci. 139 (44) (2022).
[44] J. Guo, S. Ye, H. Li, J. Song, J. Qu, Novel carbon dots with dual excitation for imaging and silver ion detection in living cells, Dyes Pigments 183 (2020), 108723.
[45] F. Yan, H. Zhang, N. Yu, Z. Sun, L. Chen, Conjugate area-controlled synthesis of multiple-color carbon dots and application in sensors and optoelectronic devices, Sens. Actuators, A B329 (2021), 129263.
[46] L. Li, L. Shi, J. Jia, O. Eltayeb, W. Lu, Y. Tang, et al., Dual photoluminescence emission carbon dots for ratiometric fluorescent GSH sensing and cancer cell recognition, ACS Appl. Mater. Interfaces 12 (2020) 18250–18257.
[47] J. Li, Y. Wang, S. Sun, A.M. Lv, K. Jiang, Y. Li, et al., Disulfide bond-based self-crosslinked carbon-dots for turn-on fluorescence imaging of GSH in living cells, Analyst 145 (2020) 2982–2987.
[48] D. Wang, Y.-t. Meng, Y. Zhang, Q. Wang, W.-j. Lu, S.-m. Shuang, et al., A specific discriminating GSH from Cys/Hcy fluorescence nanosensor: the carbon dots-MnO2 nanocomposites, Sens. Actuators, B 367 (2022), 132135.
[49] W. Dong, R. Wang, X. Gong, C. Dong, An efficient turn-on fluorescence biosensor for the detection of glutathione based on FRET between N,S dual-doped carbon dots and gold nanoparticles, Anal. Bioanal. Chem. 411 (2019) 6687–6695.
[50] Y. Meng, Q. Guo, Y. Jiao, P. Lei, S. Shuang, C. Dong, Smartphone-based label-free ratiometric fluorescence detection of sertraline and glutathione based on the use of orange-emission carbon dots, Mater. Today Chem. 26 (2022), 101170.
[51] Q.Y. Cai, J. Li, J. Ge, L. Zhang, Y.L. Hu, Z.H. Li, et al., A rapid fluorescence "switch-on" assay for glutathione detection by using carbon dots-MnO2 nanocomposites, Biosens. Bioelectron. 72 (2015) 31–36.
[52] Z. Song, F. Quan, Y. Xu, M. Liu, L. Cui, J. Liu, Multifunctional N,S co-doped carbon quantum dots with pH- and thermo-dependent switchable fluorescent properties and highly selective detection of glutathione, Carbon 104 (2016) 169–178.
[53] R. Jia, K. Jin, J. Zhang, X. Zheng, S. Wang, J. Zhang, Colorimetric and fluorescent detection of glutathione over cysteine and homocysteine with red-emitting N-doped carbon dots, Sens. Actuators, B 321 (2020), 128506.
[54] F. Zu, F. Yan, Z. Bai, J. Xu, Y. Wang, Y. Huang, X. Zhou, The quenching of the fluorescence of carbon dots: a review on mechanisms and applications, Microchim. Acta 184 (7) (2017) 1899–1914.
[55] J. An, G. Liu, M. Chen, Y. Hu, R. Chen, Y. Lyu, C. Zhang, Y. Liu, One-step synthesis of fluorescence-enhanced carbon dots for Fe (III) on-off-on sensing, bioimaging and light-emitting devices, Nanotechnology 32 (28) (2021), 285501.
[56] Y. Zhang, Z. Gao, W. Zhang, W. Wang, J. Chang, J. Kai, Fluorescent carbon dots as nanoprobe for determination of lidocaine hydrochloride, Sens. Actuators, B 262 (2018) 928–937.
[57] J. Yue, L. Li, L. Cao, M. Zan, D. Yang, Z. Wang, Z. Chang, Q. Mei, P. Miao, W. F. Dong, Two-step hydrothermal preparation of carbon dots for calcium ion detection, ACS Appl. Mater. Interfaces 112 (47) (2019) 44566–44572.